Numer Algor (2015) 70:43–59
DOI 10.1007/s11075-014-9934-9

ORIGINAL PAPER

Series solutions of non-similarity boundary layer flows of nano-fluids over stretching surfaces

U. Farooq · T. Hayat · A. Alsaedi · S. J. Liao

Received: 10 June 2014 / Accepted: 16 October 2014 / Published online: 14 November 2014

Abstract In this paper the convergent series solutions for the non-similarity flow of viscous fluid with nanoparticles are given. Fundamental equations employed in the mathematical modelling include the novel aspects of Brownian motion and thermophoresis. Non-similarity flow is induced by a stretching sheet with arbitrary velocity. The so-called homotopy analysis method (HAM) is applied to gain the convergent series solutions of the nonlinear partial differential equation. It is noticed that flow field, temperature and nanoparticle volume fraction profile are greatly influenced by the physical parameters such as Prandtl number, Brownian motion parameter, thermophoresis parameter and Lewis number. To the best of our knowledge, the present analysis seems to be a first attempt to non-similarity boundary layer flows of viscous fluids with nanoparticles.

Keywords Non-similarity flow · Nanofluid · Convergent analytic solution · Homotopy analysis method (HAM)

U. Farooq · S. J. Liao
State Key Laboratory of Ocean Engineering, School of Naval Architecture, Ocean and Civil Engineering, Shanghai Jiao Tong University, Shanghai 200240, China

T. Hayat
Department of Mathematics, Quaid.i.Azam University, Islamabad 44000, Pakistan

T. Hayat · A. Alsaedi · S. J. Liao (✉)
Nonlinear Analysis and Applied Mathematics (NAAM) Research Group, Faculty of Science, King Abdulaziz University, P.O. Box 80203, Jeddah, 21589, Saudi Arabia
e-mail: sjliao@sjtu.edu.cn

1 Introduction

The study of boundary layer flow by stretching sheet has received a great deal of research interest due to its wide applications in metallurgy, extrusion processes, cooling of an infinite metallic plate in a cooling bath, melt spinning, hot rolling, manufacture of plastic and rubber sheets, food processing, movement of biological fluids, cooling or drying of papers and in textile and glass fiber production. Both the rates of stretching and cooling have pivotal role for quality of the end product with desired characteristics. Crane [1] initiated the analysis of two-dimensional similar flow of viscous fluid over a surface with linear stretching velocity. He obtained the closed form solution of the resulting nonlinear mathematical problem. Afterwards extensive literature is now available on this topic through different aspects of suction/injection, magnetohydrodynamics (MHD), rheological characteristics, heat and mass transfer, chemical reaction etc. Information is replete especially to the similar boundary layer flows of viscous fluid in this direction. Some recent contributions on the title may be mentioned by the studies [2, 5]. The non-similarity flows have not been discussed extensively in the past. Only few attempts addressed such flows for viscous and second order fluids. For instance Liao [6] analyzed non-similarity boundary layer flow of viscous fluid bounded by a stretching sheet. Non-similar solution for boundary layer flow of second order fluid over a stretching surface with arbitrary velocity was provided by You et al. [7]. Non-similar natural convection flow of viscous fluid over a permeable sheet is examined by Kousar and Liao [8]. Nakhchi et al. [9] addressed the non-similarity thermal boundary layer flow over a stretching flat plate. Kousar and Mahmood [10] examined non-similarity boundary layer flow of viscous fluid by a porous wedge.

The thermal load removal at present is a serious concern in power, manufacturing, transportation, chemical and electronic industries. Although several mechanisms have been suggested for cooling the high heat flux surfaces but majority of such mechanisms depend upon fluid suction/injection structure variation, heated surface vibration etc. Such mechanisms are not useful especially for cooling requirement of future generation of microelectronic systems. This is because of the reason that such heat transfer mechanisms result in undesirable cooling system size and low efficiency of heat exchangers. Concept of nanofluids are considered feasible to obviate this problem. Thus the topic of nanofluids has attracted the attention of recent scientists and engineers. In fact the usual fluids in view of their low heat transfer characteristics do not posses effective heat transfer capabilities. Nanofluids is a material consisting of nanometer-sized particles. Nanofluids are engineered colloidal suspensions of nanoparticles in a base fluid. Commonly used base fluids are oil, water, lubricants, toluene, ethylene glycol, biofluids and polymer solutions whereas the nanoparticles are made of metals (gold, aluminium, copper, iron, titanium, methanol), oxides (Al_2O_3), carbides (Sic), nitride (AIN, SiN) or non-metals (Graphite, Carbon nanotubes). Sure, the selection of base fluid particle combination depends upon the application for which the nanofluid is intended. In literature, the similar boundary layer flows of nanofluid have been analyzed under different aspects (see for instance [11–23]).

The objective of present communication is to venture further in the regime of non-similarity boundary layer flows of fluids in the presence of nanoparticles. Literature survey reveals that there is no such attempt available in this direction. Thus the main theme here is to revisit the non-similarity flow of analysis of ref. [9] in the presence of nanoparticles. The flow formulation is first presented and then the resulting nonlinear differential systems are solved by optimal homotopy analysis method (OHAM). The OHAM series solutions contain the convergence-control parameters as defined by Liao [24]. It should be noticed that the convergence-control parameters are just the artificial parameters introduced in the high order deformation equations to enhance the convergence but physically they have no meaning at all. Obviously, it is very important to ensure the convergence of the approximation series and the convergence of homotopy analysis method (HAM) results greatly depends on the proper choice of convergence-control parameters. There are two standard procedures to obtain convergence-control parameters. One is through $\hbar$-curve method and the other one is called Minimum Error Method. In $\hbar$-curve method we plot a figure which displays the variations of $\hbar$ with a fixed functional value (for an example, $f''(0)$) given by any order of HAM iteration. It gives $\hbar$ region and any value from that region is reasonable to be picked. However, $\hbar$ region contains infinite values and it is quite hard to pick the best value from $\hbar$ region. In minimum error method the optimal values of the convergence-control parameters are obtained by the minimum of average squared residual error. The choice of the optimal values of the convergence-control parameters by using minimum error method as defined by Liao [25] is often referred to as OHAM and has been applied in the literature (see [26–30]). Here, the optimal values for the convergence-control parameters are obtained through the minimum of total average squared residual error. In this paper, the convergence of the OHAM series solutions has been demonstrated by an illustrative example. The effects of the physical parameters such as Pr, N_b, N_t and Le on the fluid flow, temperature distributions, concentration profiles, the local Nusselt number and the local Sherwood number are studied in detail.

2 Mathematical formulation

Here we investigate the two-dimensional flow of viscous nanofluid bounded by a stretching surface with velocity $U_w(x)$. Two different cases of $U_w(x)$ are considered. The boundary layer approximations are employed. The sheet is taken at $y = 0$ whereas x-axis is along the surface. The effects of Brownian motion and thermophoresis are accounted.

Continuity Equation

$$\frac{\partial u}{\partial x} + \frac{\partial v}{\partial y} = 0. \tag{1}$$

Momentum Equation

$$u\frac{\partial u}{\partial x} + v\frac{\partial u}{\partial y} = \nu\frac{\partial^2 u}{\partial y^2}. \tag{2}$$

Thermal energy equation

$$u\frac{\partial T}{\partial x}+v\frac{\partial T}{\partial y}=\alpha\frac{\partial^2 T}{\partial y^2}+\tau\left\{D_B\left(\frac{\partial C}{\partial y}\frac{\partial T}{\partial y}\right)+\frac{D_T}{T_\infty}\left(\frac{\partial T}{\partial y}\right)^2\right\}. \tag{3}$$

Nanoparticle volume fraction equation

$$u\frac{\partial C}{\partial x}+v\frac{\partial C}{\partial y}=D_B\left(\frac{\partial^2 C}{\partial y^2}\right)+\frac{D_T}{T_\infty}\left(\frac{\partial^2 T}{\partial y^2}\right). \tag{4}$$

In the above expressions of continuity, momentum and nanoparticle volume fraction, $\alpha=\frac{k}{(\rho c)_f}$ is the thermal diffusivity of the fluid, k is the fluid thermal conductivity, τ is the volumetric expansion coefficient of nanofluid, ν is the kinematic viscosity, T is the temperature, C is the nanoparticle fraction, D_B is the Brownian diffusion coefficient and D_T is the thermophoretic diffusion coefficient. The origin of the coordinate axes (x,y) is defined as a rest point on the stretching sheet when two forces with same magnitude are applied in different direction. Since the flow is symmetric therefore we only consider the flow in the first quadrant i.e. $x\geq 0$ and $y\geq 0$. The fluid is at rest far from the sheet (i.e., as $y\to\infty$) and the sheet exhibits stretching with velocity $U_w(x)$. Therefore the corresponding boundary conditions are

$$u=U_w(x),\ v=0,\ T=T_w,\ C=C_w \quad \text{at} \quad y=0, \tag{5}$$

and

$$u=0,\ \frac{\partial v}{\partial x}=0 \quad \text{at} \quad x=0, \tag{6}$$

$$u\to 0,\ T\to T_\infty,\ C\to C_\infty \quad \text{as} \quad y\to\infty. \tag{7}$$

The stream functions (ψ) and the non-similarity transformation (η) are defined as follows:

$$\psi=\nu^{\frac{1}{2}}\sigma(x)f(x,\eta),\ \eta=\frac{y}{\nu^{\frac{1}{2}}\sigma(x)}, \tag{8}$$

where $\sigma(x)>0$ is a real function. Using the stream function ψ we get

$$u=\frac{\partial f}{\partial \eta},\ v=-\nu^{\frac{1}{2}}\left[\sigma'(x)\left(\eta\frac{\partial f}{\partial \eta}-f\right)-\sigma(x)\frac{\partial f}{\partial x}\right]. \tag{9}$$

Without loss of generality let us consider the case $U_w(x)=U_w(\xi)$, where $\xi=\Gamma(x)$ is a given real function of x and considering

$$\theta(\eta)=\frac{T-T_\infty}{T_w-T_\infty},\ \phi(\eta)=\frac{C-C_\infty}{C_w-C_\infty}. \tag{10}$$

Substituting (8–10) into (1–4), the non-dimensional governing partial differential equations are as follows:

$$\frac{\partial^3 f}{\partial \eta^3} + \sigma_1(\xi) f \frac{\partial^2 f}{\partial \eta^2} + \sigma_2(\xi)\left(\frac{\partial f}{\partial \xi}\frac{\partial^2 f}{\partial \eta^2} - \frac{\partial f}{\partial \eta}\frac{\partial^2 f}{\partial \xi \partial \eta}\right) = 0, \quad (11)$$

$$\frac{\partial^2 \theta}{\partial \eta^2} + PrN_b \frac{\partial \phi}{\partial \eta}\frac{\partial \theta}{\partial \eta} + PrN_t \left(\frac{\partial \theta}{\partial \eta}\right)^2 + Pr\sigma_1(\xi) f \frac{\partial \theta}{\partial \eta} + Pr\sigma_2(\xi)\left(\frac{\partial f}{\partial \xi}\frac{\partial \theta}{\partial \eta} - \frac{\partial \theta}{\partial \xi}\frac{\partial f}{\partial \eta}\right) = 0, \quad (12)$$

$$\frac{\partial^2 \phi}{\partial \eta^2} + \frac{N_t}{N_b}\frac{\partial^2 \theta}{\partial \eta^2} + LePr\sigma_1(\xi) f \frac{\partial \phi}{\partial \eta} + LePr\sigma_2(\xi)\left(\frac{\partial f}{\partial \xi}\frac{\partial \phi}{\partial \eta} - \frac{\partial \phi}{\partial \xi}\frac{\partial f}{\partial \eta}\right) = 0, \quad (13)$$

In the above equations, the parameters Pr, N_b, N_t, Le and Sc are the Prandtl number, the Brownian motion parameter, the thermophoresis parameter or Lewis and Schmidt numbers respectively. These are defined by

$$N_b = \frac{\tau D_B (C_w - C_\infty)}{\nu}, \; N_t = \frac{\tau D_T (T_w - T_\infty)}{\nu T_\infty}, \; Le = \frac{Sc}{Pr}, \; Pr = \frac{\nu}{\alpha}, \; Sc = \frac{\nu}{D_B}. \quad (14)$$

Also

$$PrN_b = \frac{\tau D_B (C_w - C_\infty)}{\alpha}, \; PrN_t = \frac{\tau D_T (T_w - T_\infty)}{\alpha T_\infty}, \; LePr = Sc. \quad (15)$$

and

$$\sigma_1(\xi) = \frac{1}{2}\left[\sigma^2(x)\right]', \; \sigma_2(\xi) = \Gamma'(x)\sigma^2(x). \quad (16)$$

The corresponding boundary conditions are

$$\left.\begin{array}{lll} f(\xi,0) = 0, & f_\eta(\xi,0) = U_w(\xi), & f_\eta(\xi,\infty) = 0, \\ \theta(\xi,0) = 1, & \theta(\xi,\infty) = 0, & \\ \phi(\xi,0) = 1, & \phi(\xi,\infty) = 0. & \end{array}\right\} \quad (17)$$

Here the so-called homotopy analysis method (HAM) (for details see [6, 31, 32]) is used to provide a general approach to solve non-similarity boundary layer flows of nanofluids governed by PDE's (11–13) with boundary conditions (17). Its basic ideas and mathematical formulations are given in the Appendix. For details, please refer to Liao [6]. We point out the great freedom in HAM to choose the convergence-control parameters $\left(c_0^f, c_0^\theta, c_0^\phi\right)$, the auxiliary function $\mathcal{H}_i(\eta)(i = 1-3)$, the auxiliary linear operators $\mathcal{L}_i(i = 1-3)$, the initial approximations $(f_0(\eta), \theta_0(\eta), \phi_0(\eta))$. If all of them are so properly chosen the solutions $(f_k(\eta), \theta_k(\eta), \phi_k(\eta))$ from (34–36) of high order deformation equations can be easily obtained by means of computation software $Mathematica$. The convergence of OHAM series solutions is checked by the total average squared residual error [6, 33].

The flow, temperature distribution, concentration profile, the local Nusselt number and the local Sherwood number are analyzed for various values of the physical parameters like Prandtl number, Brownian motion parameter, thermophoresis parameter and Lewis number.

3 Results and discussion

Certainly, it is quite necessary to assure the convergence of the non-similarity OHAM series solutions. The convergence of the optimal HAM (OHAM) series solutions depends upon the convergence-control parameters. The convergence-control parameters provide us a simple way to control the convergence rate of homotopy series solution. It should be emphasized that we have great freedom to choose the value of convergence-control parameters that guarantee the convergence of the homotopy series solutions. The accuracy of the OHAM series solutions can be verified by the exact squared residual error of the governing equation (19–21) as shown in the (43–45). Since it takes too much CPU time to compute exact squared residual error even if the order of approximation is not so high. Therefore for the sake of computational efficiency, we used here the average squared residual errors (47–49).

Clearly, the total average squared residual error $\mathcal{E}_k^t\left(c_0^f, c_0^\theta, c_0^\phi\right)$ is a good approximation of total exact squared residual error $\Delta_k^t\left(c_0^f, c_0^\theta, c_0^\phi\right)$ provided the integer N in equations (47–49) is sufficiently large. We have chosen $N = 80$ throughout the computations in this paper. Since $\mathcal{E}_k^t\left(c_0^f, c_0^\theta, c_0^\phi\right)$ depends upon the convergence-control parameters therefore the smaller the value of $\mathcal{E}_k^t\left(c_0^f, c_0^\theta, c_0^\phi\right)$ the better the approximation.

The minimum value of the $\mathcal{E}_k^t\left(c_0^f, c_0^\theta, c_0^\phi\right)$ can be obtained by means of the softwares such as *Maple*, *Mathematica* and *Matlab*. Throughout in this paper, we fix $c_0^f = -0.5$ as [6] has already proved that one can get convergent HAM series solutions for (11) in the whole domain $0 \le \xi \le 1$ and $0 \le \eta \le +\infty$ (corresponding to $0 \le x \le +\infty$ and $0 \le y \le +\infty$). Without loss of genrality, let's consider the case $Pr = Le = 1.0$, $N_b = N_t = 0.1$. The optimal values of the convergence-control parameters c_0^θ and c_0^ϕ are obtained by the minimum of the $\mathcal{E}_k^t\left(c_0^f, c_0^\theta, c_0^\phi\right)$ through directly employing the command "**Minimized**" in *Mathematica*. It can be seen in Table 1 that as we increase the order of iteration the corresponding average squared residual error's are decreasing. The computation is stopped when a certain convergence criterion is satisfied. This illustrative example validates the reliability of the non-similarity HAM series solutions.

Figures 1(a) and (b) describe the local Nusselt number and the local Sherwood number as the functions of the coordinate x in the positive direction at the leading

Table 1 Average squared residual errors at different order of iterations for $Le = Pr = 1.0$, $N_b = N_t = 0.1$, $\sigma_1(x) = \frac{1}{2}$ and $\sigma_2(x) = 1 - \xi$ by using $c_0^f = -0.5$, $c_0^\theta = -0.87$ and $c_0^\theta = -1.20$

k	10	20	30
$\mathcal{E}_k^f$	1.6×10^{-5}	3.01×10^{-7}	1.20×10^{-8}
$\mathcal{E}_k^\theta$	1.0×10^{-5}	5.1×10^{-7}	3.7×10^{-8}
$\mathcal{E}_k^\phi$	1.4×10^{-5}	8.9×10^{-7}	5.8×10^{-8}
$\mathcal{E}_k^t$	4.2×10^{-5}	1.7×10^{-6}	1.0×10^{-7}

edge with different stretching velocities $U_w(x)$. The stretching velocity of the surface $U_w(x) = \frac{x}{1+x}$ increases monotonically from 0 to 1. However the solutions of the boundary value problem (1–4) subject to the boundary conditions (5–7) with surface velocities $U_w \to x$ as $x \to 0$ and $U_w \to 1$ as $x \to \infty$ can be obtained with similarity transformations $\frac{y}{\sqrt{\nu}}$ and $\frac{y}{\sqrt{\nu x}}$, respectively. The direct study of the boundary layer flows with nanoparticles for the stretching surfaces under non-similarity transformations is important in the sense how we can develop the relationships between the heat and mass transfer for both similarity and non-similarity transformations. It is reasonable to consider $\sigma(x) = \sqrt{1+x}$ under the definition of η in (10). For the sake of simplicity, when $U_w(x) = \frac{x}{1+x}$ we define $\xi = \Gamma(x) = \frac{x}{x+1}$ which gives $U_w(\xi) = \xi$, $\sigma_1(\xi) = \frac{1}{2}$, $\sigma_2(\xi) = 1 - \xi$. Then the local Nusselt number and the local Sherwood number are $\nu^{\frac{1}{2}} Nu_x = -\frac{x\theta'(\xi,0)}{\sigma(x)}$ and $\nu^{\frac{1}{2}} Sh_x = -\frac{x\phi'(\xi,0)}{\sigma(x)}$, respectively. When $U_w(x) = x$ we define $\xi = x$ which gives the local Nusselt number $\nu^{\frac{1}{2}} Nu_x = -x\theta'(\xi, 0)$ and the local Sherwood number $\nu^{\frac{1}{2}} Sh_x = -x\phi'(\xi, 0)$. When $U_w(x) = 1$ the local Nusselt number and the local Sherwood number is defined as $\nu^{\frac{1}{2}} Nu_x = -x^{\frac{1}{2}}\theta'(\xi, 0)$ and $\nu^{\frac{1}{2}} Sh_x = -x^{\frac{1}{2}}\phi'(\xi, 0)$. It is observed from Figs. 1(a) and (b) that the local Nusselt number and the local Sherwood number increase in the positive x-direction for boundary layer flows with nanoparticles under similarity and non-similarity transformations for different stretching velocities. The magnitude of local Nusselt number and the local Sherwood number for the surface with $U_w(x) = 1$ when $x < 1$ is higher than the surfaces with $U_w(x) = \frac{x}{1+x}$ and $U_w(x) = x$. However for the surface with $U_w(x) = \frac{x}{1+x}$ and $U_w(x) = x$ the local Nusselt number and the local Sherwood number is same at the leading edge when $x \to 0$. The magnitude of the local Nusselt number and the local Sherwood number for $U_w(x) = \frac{x}{1+x}$ when $x >> 1$ is higher than $U_w(x) = x$ and $U_w(x) = 1$. Since the process of heat and

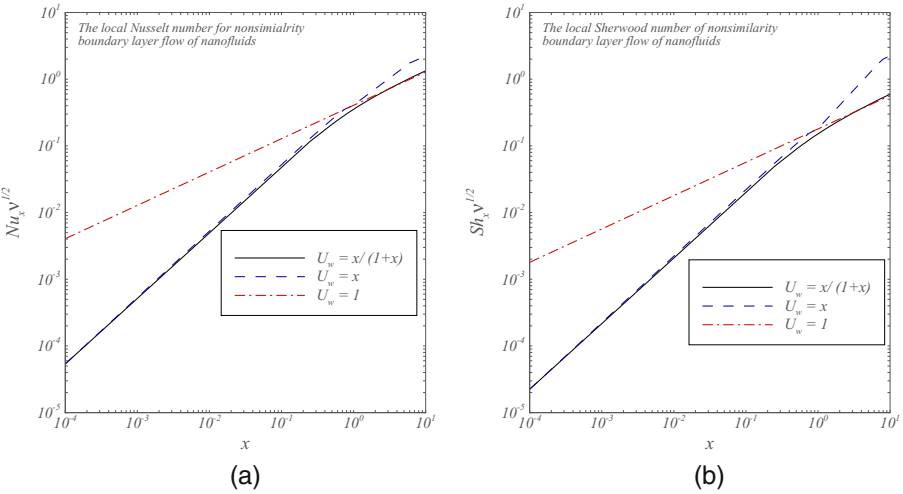

Fig. 1 (**a**) The local Nusselt number (**b**) The local Sherwood number

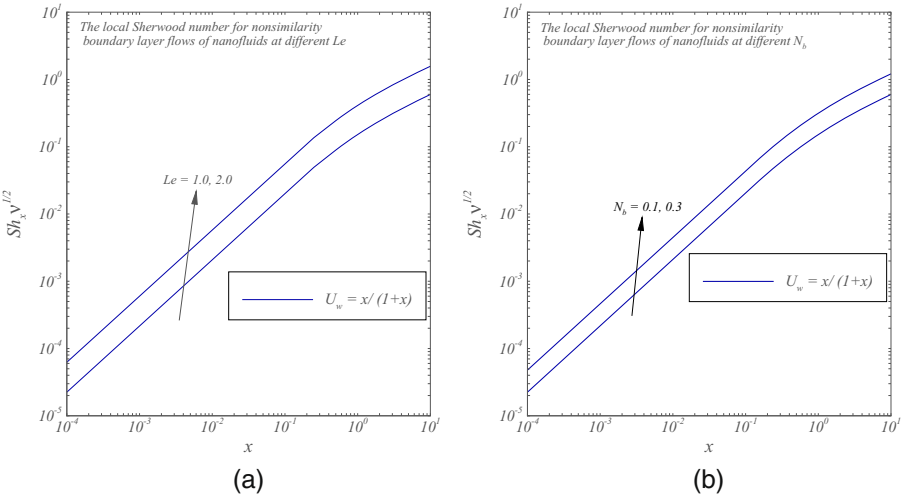

Fig. 2 (**a**) Graph of the local Sherwood number for different Le (**b**) Graph of the local Sherwood number for different N_b

mass transfer are analogous to each other as it can be seen in the Figs. 1(a) and (b), therefore it is easy to develop an understanding of mass transfer.

Figure 2(a) shows the influence of the Le on the local Sherwood number for $U_w(x) = \frac{x}{1+x}$. It should be noticed that $Sc \approx 1$ indicates that (13) and (11) coincide with each other. Similarly if we replace Sc by $Pr.Le$ in (13), it represents that relative heat and mass transfer by diffusion is comparable. The increase in Le means a larger thermal diffusivity which is a result of higher thermal conductivity or low heat capacity. The conduction increases and thus the temperature enhances. The higher thermal diffusivity means high rate of heat transfer and since the process of heat and mass transfer undergoes simultaneously especially in gases therefore it can be seen in Fig. 2(a) that the increase in Le enhances the local Sherwood number.

Figure 2(b) represents the effect of N_b on the local Sherwood number. The Brownian motion is considered to be an important phenomenon in nanofluids because the effective thermal conductivity of nanofluids does not depend only on the structure of the nanoparticles but also on the movement of nanoparticles in base fluid. Figure 2(b) demonstrates that the increase in N_b yields enhancement in the mass diffusion which results in the increase in mass transfer.

The local Nusselt number at different locations of x for various values of Pr is shown in Fig. 3(a). It can be seen the increase in Pr increases the local Nusselt number however the effects of Pr are significant when $x > 1$.

The buildup of velocity profiles of the boundary layer flow for stretching surface for increasing values of ξ is shown in Fig. 3(b). It is observed that at the leading edge the velocity profiles increase proportionally with the increasing values of ξ. The velocity gradient decreases in the downstream direction and velocity profiles for increasing ξ become constant in the free stream region.

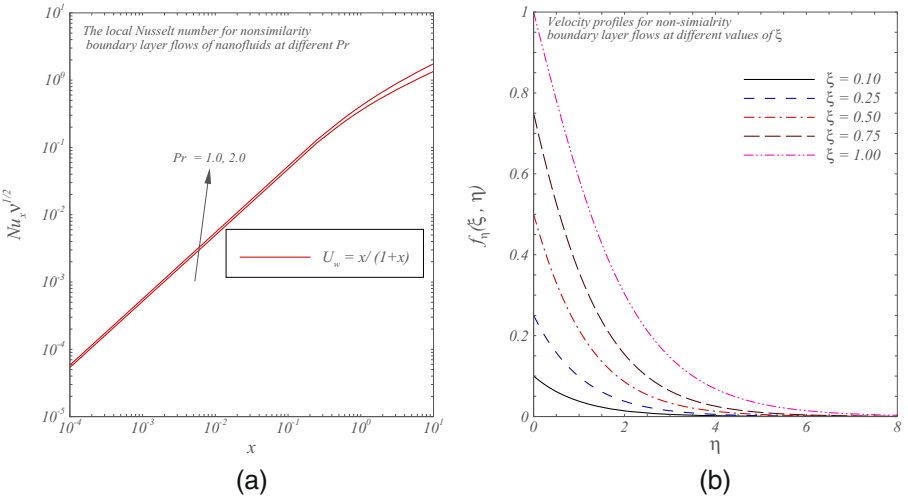

Fig. 3 (**a**) Graphs of the local Nusselt number for different Pr. (**b**) Graphs of the velocity profiles for various ξ.

The dimensionless temperature profiles for a surface stretching with velocity U_w are shown in Fig. 4(a). At the leading edge of the surface, the fluid temperature is equal to the surface temperature and gradually decreases to the temperature of the surrounding fluid and sufficiently far away from the surface it asymptotically approaches to zero. The effect of the increase in the values ξ is to increase the temperature in the surrounding fluid.

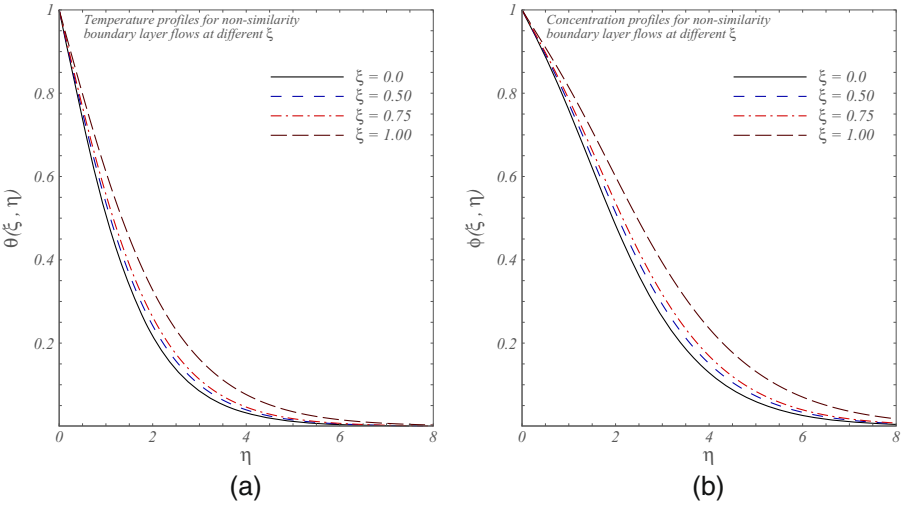

Fig. 4 (**a**) Temperature profiles for various values of ξ. (**b**) Concentration profiles for various values of ξ

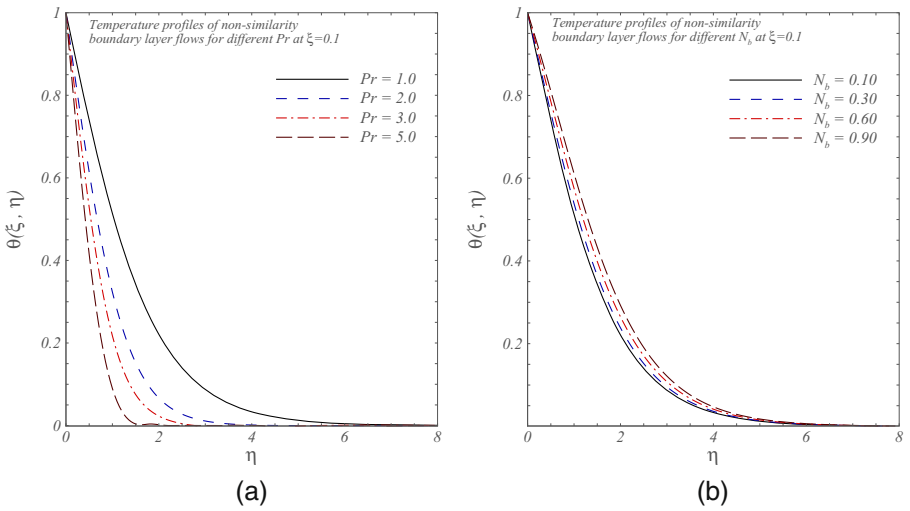

Fig. 5 (**a**) Temperature profiles for various values of Pr (**b**)Temperature profiles for various values of N_b

The dimensionless concentration profile in Fig. 4(b) under the boundary conditions for specified values of ξ depicts that concentration is highest at the leading edge and it gradually decreases to low concentration with the increase in the values of η. Increase in the values of ξ exhibits an increase to the concentration in the boundary layer region. Figure 5(a) shows variations of Pr on the temperature profiles at a fixed value of ξ keeping all other physical parameters constant. The Pr is increased which is due to the relatively low thermal diffusivity (thermal conductivity), the reduced conduction decreases the thermal boundary layer thickness. Therefore the temperature of a nanofluids are strong function of Pr. It is illustrated in Fig. 5(a) the temperature decreases with Pr in the boundary layer region.

Nanofluids are dynamic systems so the effects of Brownian motion mechanism in the enhancement of temperature through particle-particle collision caused by Brownian motion of nanoparticles are shown in Fig. 5(b). It shows that purely increasing Brownian motion of nanoparticles enhances the temperature in the boundary layer region. Similarly Fig. 6(a) demonstrates the variation of temperature profile with respect to the change of N_t keeping all other parameters fixed. It can be seen that the increase in N_t also increases the temperature profile in the boundary layer region.

Figure 6(b) shows variations of nanofluid concentration graph via Le. Here the concentration is a decreasing function of Le. Physically it validates the fact that the increase in the Le reduces the mass diffusivity therefore mass transfer slows down through the fluid because the fluid conducts heat slowly relative to its volumetric heat capacity.

Figures 7(a) and (b) indicate the nanofluid concentration with respect to different variations of N_b and N_t, respectively. Figure 7(a) indicates that the effect of N_b on nanoparticle concentration is to decrease the concentration profile. Figure 7(b) witnesses that the increase in N_t increases the concentration in the boundary layer region. The concentration profile is strictly decreasing when $N_t = 0.10$. However

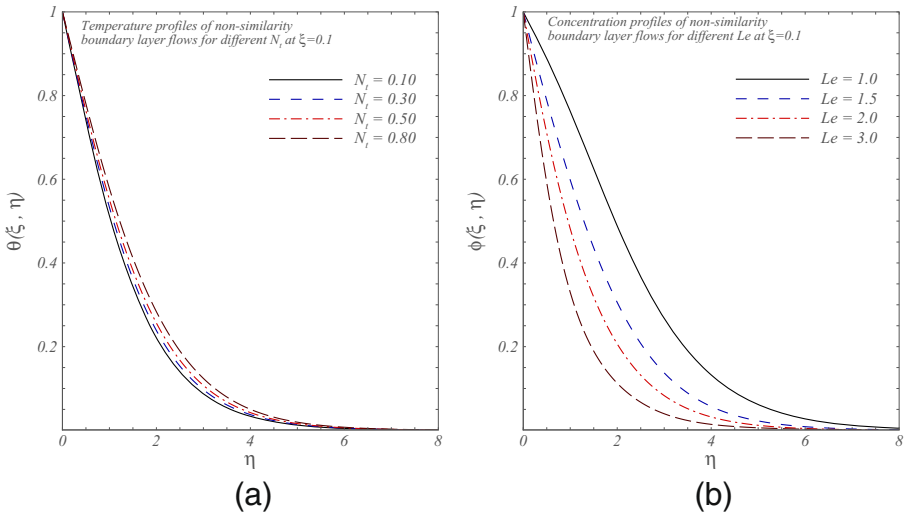

Fig. 6 (**a**) Temperature profiles for various values of N_t (**b**) Concentration profiles for various values of Le

the concentration shootout is observed for $N_t = 0.3, 0.5, 0.8$ i.e. the concentration is initially increasing and then it starts decreasing. The peak value of the concentration increases significantly with the increase in N_t and then it starts decreasing.

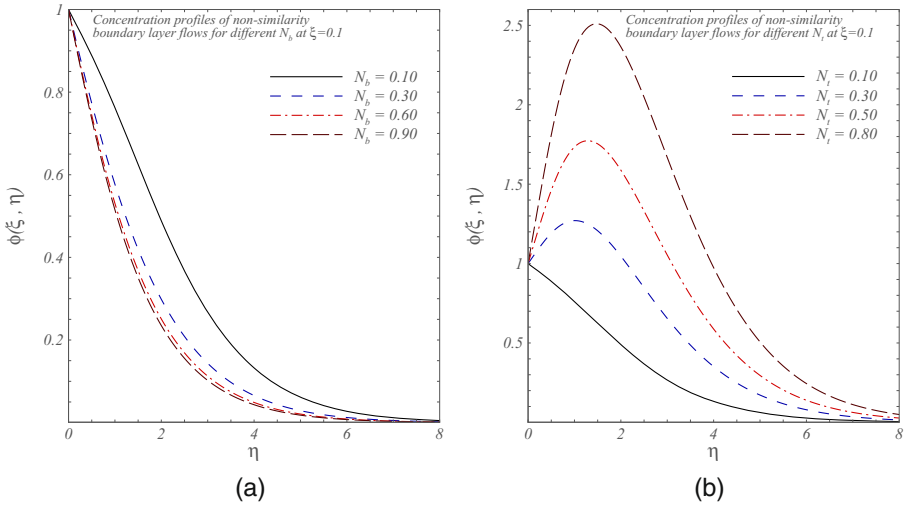

Fig. 7 (**a**) Concentration profiles for various values of N_b (b) Concentration profiles for various values of N_t

4 Conclusions

In this paper, an analytic approach based on optimal homotopy analysis method (OHAM) is proposed to obtain convergent series solutions for the non-similarity boundary layer flows of nanofluids. The series solutions of the resulting partial differential equations through non-similar transformations are obtained by OHAM. The convergence criterion of the OHAM series solutions is satisfied through average squared residual errors. It is found that for the non-similarity boundary layer flow of a surface stretching with velocity $U_w = \frac{x}{1+x}$ the so-called local similarity exists only near $x = 0$ i.e. $U_w = x$ and $x = +\infty$ i.e. $U_w = 1$. The effects of the non-similarity variable ξ and various values of the physical parameters such as N_b, N_t, Pr and Le on the fluid velocity, temperature, concentration profile, the local Nusselt number and Sherwood number are illustrated through graphs. We may extract some important findings from the presented analysis as follows:

- The increase in the values of x increases the local Nusselt and the local Sherwood numbers. Keeping all other parameters fixed the stretching velocities $U_w = \frac{x}{1+x}$ and $U_w = x$ the local Sherwood number and the local Nuseelt number are same when $x << 1$.
- Effects of Le and N_b are to increase the local Sherwood number.
- An increase in the Prandtl number gives rise to the local Nusselt number.
- The velocity profiles increase proportionally with ξ at the leading edge. Also the increase in the values of ξ enhances both the temperature and concentration profiles .
- Larger Prandtl number decreases the temperature whereas the temperature profiles increase when the values of N_b and N_t are increased.
- Increase in the values of the parameters Le and N_b significantly decreases the concentration profiles and the increase in the values of N_t enhances the concentration profiles.

Acknowledgments This work is supported in part by State Key Laboratory of Ocean Engineering (Approval No. GKZD010063), National Natural Science Foundation of China (Approval No. 11272209 and No. 51209136) and the Deanship of Scientific Research (DSR), King Abdulaziz University, Saudi Arabia (Grant No. 37-130-35-HiCi).

Appendix Approach based on the HAM

We apply the OHAM to solve the system of nonlinear ordinary differential equation (11–13) with boundary conditions (17). In the framework of the OHAM the solutions for $f(\eta)$, $\theta(\eta)$ and $\phi(\eta)$ can be expressed explicitly by an infinite number of sub-functions in the following forms:

$$f(\eta) = \sum_{k=0}^{+\infty} f_k(\eta),\ \theta(\eta) = \sum_{k=0}^{+\infty} \theta_k(\eta),\ \phi(\eta) = \sum_{k=0}^{+\infty} \phi_k(\eta) \tag{18}$$

$$\mathcal{N}_1[f(\xi,\eta),\theta(\xi,\eta),\phi(\xi,\eta)] = \frac{\partial^3 f}{\partial \eta^3} + \sigma_1(\xi) f \frac{\partial^2 f}{\partial \eta^2} + \sigma_2(\xi)\left(\frac{\partial f}{\partial \xi}\frac{\partial^2 f}{\partial \eta^2} - \frac{\partial f}{\partial \eta}\frac{\partial^2 f}{\partial \xi \partial \eta}\right), \quad (19)$$

$$\mathcal{N}_2[f(\xi,\eta),\theta(\xi,\eta),\phi(\xi,\eta)] = \frac{1}{Pr}\frac{\partial^2 \theta}{\partial \eta^2} + N_b \frac{\partial \phi}{\partial \eta}\frac{\partial \theta}{\partial \eta} + N_t\left(\frac{\partial \theta}{\partial \eta}\right)^2 + \sigma_1(\xi) f \frac{\partial \theta}{\partial \eta} + \sigma_2(\xi)\left(\frac{\partial f}{\partial \xi}\frac{\partial \theta}{\partial \eta} - \frac{\partial \theta}{\partial \xi}\frac{\partial f}{\partial \eta}\right), \quad (20)$$

$$\mathcal{N}_3[f(\xi,\eta),\theta(\xi,\eta),\phi(\xi,\eta)] = \frac{\partial^2 \phi}{\partial \eta^2} + \frac{N_t}{N_b}\frac{\partial^2 \theta}{\partial \eta^2} + Le.\sigma_1(\xi) f \frac{\partial \phi}{\partial \eta} + Pr.Le.\sigma_2(\xi)\left(\frac{\partial f}{\partial \xi}\frac{\partial \phi}{\partial \eta} - \frac{\partial \phi}{\partial \xi}\frac{\partial f}{\partial \eta}\right). \quad (21)$$

From physical points of view, it is clear that all the solutions should be in the form as given below therefore

$$f(\eta) = A^k_{0,0} + \sum_{k=0}^{+\infty}\sum_{j=1}^{+\infty}\sum_{i=0}^{+\infty} A^k_{i,j}\,\eta^i \exp(-j\eta), \quad (22)$$

$$\theta(\eta) = \sum_{k=0}^{+\infty}\sum_{j=1}^{+\infty}\sum_{i=0}^{+\infty} B^k_{i,j}\,\eta^i \exp(-j\eta), \quad (23)$$

$$\phi(\eta) = \sum_{k=0}^{+\infty}\sum_{j=1}^{+\infty}\sum_{i=0}^{+\infty} C^k_{i,j}\,\eta^i \exp(-j\eta), \quad (24)$$

where $A^k_{i,j}$, $B^k_{i,j}$ and $C^k_{i,j}$ are constant coefficients to be determined. In the OHAM, one has great freedom for the choice of the auxiliary linear operator. Thus, we can choose auxiliary linear operators as

$$\mathcal{L}_1[f(\xi,\eta)] = \frac{\partial^3 f}{\partial \eta^3} - \frac{\partial f}{\partial \eta}, \quad (25)$$

$$\mathcal{L}_2[\theta(\xi,\eta)] = \frac{\partial^2 \theta}{\partial \eta^2} - \theta, \quad (26)$$

$$\mathcal{L}_3[\phi(\xi,\eta)] = \frac{\partial^2 \phi}{\partial \eta^2} - \phi, \quad (27)$$

The auxiliary linear operators (25), (26) and (27) satisfy the following properties

$$\mathcal{L}_1[C_1 + C_2\exp(-\eta) + C_3\exp(\eta)] = 0, \quad (28)$$

$$\mathcal{L}_2[C_4 + C_5\exp(-\eta)] = 0, \quad (29)$$

$$\mathcal{L}_3[C_6 + C_7\exp(-\eta)] = 0, \quad (30)$$

where C_1, C_2, C_3, C_4, C_5, C_6 and C_7 are constants to be determined later. The corresponding auxiliary linear operator for $f(\eta)$, $\theta(\eta)$ and $\phi(\eta)$ are $\mathcal{L}_1$, $\mathcal{L}_2$ and $\mathcal{L}_3$, respectively.

In OHAM, we also have freedom to choose the initial approximations. Note that, all the initial approximations need to satisfy the boundary conditions (17). Without loss of generality, we set

$$f_0(\xi,\eta) = U_w(\xi).(1-\exp(-\eta)), \tag{31}$$
$$\theta_0(\xi,\eta) = \exp(-\eta), \tag{32}$$
$$\phi_0(\xi,\eta) = \exp(-\eta). \tag{33}$$

Thus in the frame of HAM the *k-th* order approximation $f_k(\eta)$, $\theta_k(\eta)$ and $\phi_k(\eta)$ can be obtained using the following recursive formulae

$$f_k(\xi,\eta) = \chi_k f_{k-1}(\xi,\eta) + f_k^*(\xi,\eta) + C_1^k + C_2^k e^{\eta} + C_3^k e^{-\eta}, \tag{34}$$
$$\theta_k(\xi,\eta) = \chi_k \theta_{k-1}(\xi,\eta) + \theta_k^*(\xi,\eta) + C_4^k + C_5^k e^{-\eta}, \tag{35}$$
$$\phi_k(\xi,\eta) = \chi_k \phi_{k-1}(\xi,\eta) + \phi_k^*(\xi,\eta) + C_6^k + C_7^k e^{-\eta}, \tag{36}$$

where

$$\chi_m = \begin{cases} 0, & m \le 1 \\ 1, & m > 1, \end{cases} \tag{37}$$

$C_1^k, C_2^k, C_3^k, C_4^k, C_5^k, C_6^k$, and C_7^k are integral constants determined as

$$C_1^k = -f_k^{*'}(0) - f_k^*(0),\ C_2^k = f_k^{*'}(\xi,0),\ C_3^k = 0,$$
$$C_4^k = 0,\ C_5^k = -\theta_k^*(\xi,0),\ C_6^k = 0,\ C_7^k = -\phi_k^*(\xi,0) \tag{38}$$

and $f_k^*(\xi,\eta)$, $\theta_k^*(\xi,\eta)$ and $\phi_k^*(\xi,\eta)$ are particular solutions defined by

$$f_k^*(\xi,\eta) = \mathcal{L}_1^{-1}\left[c_0^f R_k^f\right],\ \theta_k^*(\xi,\eta) = \mathcal{L}_2^{-1}\left[c_0^\theta R_k^\theta\right],\ \phi_k^*(\xi,\eta) = \mathcal{L}_3^{-1}\left[c_0^\phi R_k^\phi\right] \tag{39}$$

c_0^f, c_0^θ and c_0^ϕ are convergence-control parameters, R_k^f, R_k^θ and R_k^ϕ are defined based on (10–13) for details see Liao [34]

$$\begin{aligned} R_m^f &= \frac{1}{(m-1)!}\left.\frac{\partial^{m-1}\mathcal{N}_1\left[F(\xi,\eta;q),\Theta_1(\xi,\eta;q),\Theta_1(\xi,\eta;q)\right]}{\partial q^{m-1}}\right|_{q=0} \\ &= \frac{\partial^3 f_{m-1}}{\partial\eta^3} + \sigma_1(\xi)\sum_{n=0}^{m-1} f_{m-1-n}\frac{\partial^2 f_n}{\partial\eta^2} \\ &\quad +\sigma_2(\xi)\sum_{n=0}^{m-1}\left(\frac{\partial f_n}{\partial\xi}\frac{\partial^2 f_{m-1-n}}{\partial\eta^2} - \frac{\partial f_n}{\partial\eta}\frac{\partial^2 f_{m-1-n}}{\partial\xi\partial\eta}\right), \end{aligned} \tag{40}$$

$$\begin{aligned} R_m^\theta &= \frac{1}{(m-1)!}\left.\frac{\partial^{m-1}\mathcal{N}_2\left[F(\xi,\eta;q),\Theta_1(\xi,\eta;q),\Theta_1(\xi,\eta;q)\right]}{\partial q^{m-1}}\right|_{q=0} \\ &= \frac{\partial^2\theta_{m-1}}{\partial\eta^2} + Pr.N_b\sum_{n=0}^{m-1}\frac{\partial\phi_{m-1-n}}{\partial\eta}\frac{\partial\theta_n}{\partial\eta} + Pr.N_t\sum_{n=0}^{m-1}\left(\frac{\partial\theta_{m-1-n}}{\partial\eta}\frac{\partial\theta_n}{\partial\eta}\right) + Pr.\sigma_1(\xi) \\ &\quad \sum_{n=0}^{m-1} f_{m-1-n}\frac{\partial\theta_n}{\partial\eta} + Pr.\sigma_2(\xi)\sum_{n=0}^{m-1}\left(\frac{\partial f_m - 1 - n}{\partial\xi}\frac{\partial\theta_n}{\partial\eta} - \sum_{n=0}^{m-1}\frac{\partial\theta_{m-1-n}}{\partial\xi}\frac{\partial f_n}{\partial\eta}\right), \end{aligned} \tag{41}$$

$$R_m^{\phi} = \frac{1}{(m-1)!} \left. \frac{\partial^{m-1} \mathcal{N}_3[F(\xi,\eta;q), \Theta_1(\xi,\eta;q), \Theta_1(\xi,\eta;q)]}{\partial q^{m-1}} \right|_{q=0}$$
$$= \frac{\partial^2 \phi_{m-1}}{\partial \eta^2} + \frac{N_t}{N_b} \frac{\partial^2 \theta_{m-1}}{\partial \eta} + Pr.Le.\sigma_1(\xi) \sum_{n=0}^{m-1} f_{m-1-n} \frac{\partial \phi_n}{\partial \eta} +$$
$$+ Pr.Le.\sigma_2(\xi) \sum_{n=0}^{m-1} \left(\frac{\partial f_{m-1-n}}{\partial \xi} \frac{\partial \phi_n}{\partial \eta} - \sum_{n=0}^{m-1} \frac{\partial \phi_{m-1-n}}{\partial \xi} \frac{\partial f_n}{\partial \eta} \right). \quad (42)$$

Using the above recursive formulae, we can get the explicit analytical approximations of $f_k(\xi,\eta)$, $\theta_k(\xi,\eta)$ and $\phi_k(\xi,\eta)$ for $k = 1, 2, 3, ...$

At the kth-order of approximation, the exact squared residual error of the governing (19–21) is defined as

$$\Delta_k^f \left(c_0^f, c_0^\theta, c_0^\phi\right) = \int_0^\infty \left[\mathcal{N}_f \left(\sum_{i=0}^k f_i, \sum_{i=0}^k \theta_i, \sum_{i=0}^k \phi_i \right) \right]^2 \mathrm{d}\eta, \quad (43)$$

$$\Delta_k^\theta \left(c_0^f, c_0^\theta, c_0^\phi\right) = \int_0^\infty \left[\mathcal{N}_\theta \left(\sum_{i=0}^k f_i, \sum_{i=0}^k \theta_i, \sum_{i=0}^k \phi_i \right) \right]^2 \mathrm{d}\eta, \quad (44)$$

$$\Delta_k^\phi \left(c_0^f, c_0^\theta, c_0^\phi\right) = \int_0^\infty \left[\mathcal{N}_\phi \left(\sum_{i=0}^k f_i, \sum_{i=0}^k \theta_i, \sum_{i=0}^k \phi_i \right) \right]^2 \mathrm{d}\eta. \quad (45)$$

We define

$$\Delta_k^t \left(c_0^f, c_0^\theta, c_0^\phi\right) = \Delta_k^f \left(c_0^f, c_0^\theta, c_0^\phi\right) + \Delta_k^\theta \left(c_0^f, c_0^\theta, c_0^\phi\right) + \Delta_k^\phi \left(c_0^f, c_0^\theta, c_0^\phi\right), \quad (46)$$

where Δ_k^t is the total average squared residual error.

It is observed that much CPU time is required to calculate the exact squared residual error even if the order of approximation is not very high. Thus, to greatly decrease the CPU time, it is used here the so-called average residual error defined by

$$\mathcal{E}_k^f \left(c_0^f, c_0^\theta, c_0^\phi\right) = \frac{1}{N+1} \sum_{j=0}^N \left[\mathcal{N}_f \left(\sum_{i=0}^k f_i, \sum_{i=0}^k \theta_i, \sum_{i=0}^k \phi_i \right) \Big|_{\xi = p\delta\eta, \eta = j\delta\eta} \right]^2, \quad (47)$$

$$\mathcal{E}_k^\theta \left(c_0^f, c_0^\theta, c_0^\phi\right) = \frac{1}{N+1} \sum_{j=0}^N \left[\mathcal{N}_\theta \left(\sum_{i=0}^k f_i, \sum_{i=0}^k \theta_i, \sum_{i=0}^k \phi_i \right) \Big|_{\xi = p\delta\eta, \eta = j\delta\eta} \right]^2, \quad (48)$$

$$\mathcal{E}_k^\phi \left(c_0^f, c_0^\theta, c_0^\phi\right) = \frac{1}{N+1} \sum_{j=0}^N \left[\mathcal{N}_\phi \left(\sum_{i=0}^k f_i, \sum_{i=0}^k \theta_i, \sum_{i=0}^k \phi_i \right) \Big|_{\xi = p\delta\eta, \eta = j\delta\eta} \right]^2, \quad (49)$$

where N is an integer. It is reasonable to set $N = 80$ and $\delta\eta = 0.1$. We define

$$\mathcal{E}_k^t \left(c_0^f, c_0^\theta, c_0^\phi\right) = \mathcal{E}_k^f \left(c_0^f, c_0^\theta, c_0^\phi\right) + \mathcal{E}_k^\theta \left(c_0^f, c_0^\theta, c_0^\phi\right) + \mathcal{E}_k^\phi \left(c_0^f, c_0^\theta, c_0^\phi\right), \quad (50)$$

where $\mathcal{E}_k^t$ is the total average squared residual error. Obviously, the smaller the value of $\mathcal{E}_k^t\left(c_0^f, c_0^\theta, c_0^\phi\right)$ for given iteration k, the better the approximation. The OHAM series solutions which depend on optimal convergence-control parameters can be obtained accurately by the proper choice of convergence-control parameters.

References

1. Crane, L.J.: Flow past a stretching sheet. Z. Angew. Math. Phys. (ZAMP) **21**, 645–647 (1970)
2. Rashidi, M.M., Abelman, S., Mehr, N.F.: Entropy generation in a steady MHD flow due to a rotating porous disk in a nanofluid. Int. J. Heat Mass Transfer **62**, 515–525 (2013)
3. Turkyilmazoglu, M.: Dual and triple solutions for MHD slip flow of non-Newtonian fluid over a shrinking surface. Comput. Fluids **70**, 53–58 (2012)
4. Mukhopadhyay, S., Gorla, S.R.: Unsteady MHD boundary layer flow of an upper convected Maxwell fluid past a stretching sheet with first order constructive/destructive chemical reaction. J. Naval Architecture Eng. **9**, 123–133 (2012)
5. Hayat, T., Shehzad, S.A., Qasim, M., Obaidat, S.: Radiative flow of Jeffery fluid in a porous medium with power law heat flux and heat source. Nucl. Eng. Des. **243**, 15–19 (2012)
6. Liao, S.J.: A general approach to get series solution of non-similarity boundary-layer flows. J. Commun. Nonlinear Sci. Nummer. Simulat. **14**, 2144–2159 (2009)
7. You, X.Ch., Xu, H., Liao, S.J.: On the nonsimilarity boundary-layer flows of second-order fluids over a stretching sheet, ASME. J. Applied Mechanics **77** (2010). doi:10.1115/1.3173764
8. Kousar, N., Liao, S.J.: Series solution of non-similarity natural convection boundary-layer flows over permeable vertical surface. Sci. China Ser. G Phys. Mech. Astron. **53**(2), 360–368 (2010)
9. Nakhehi, M.E., Nobari, M.R.H., Tabrizi, H.B.: Non-similarity thermal boundary layer flow over a stretching flat plate. Chinese Phys. Letters **29**(10), 104703 (2012)
10. Kousar, N., Mahmood, R.: Series solution of non-similarity boundary-layer flow in porous medium. J. Applied Mathematics **4**, 127–136 (2013)
11. Makinde, O.D., Aziz, A.: Boundary layer flow of a nanofluid past a stretching sheet with a convective boundary condition. Int. J. Thermal Sci. **50**, 1326–1332 (2011)
12. Alsaedi, A., Awais, M., Hayat, T.: Effects of heat generation/absorption on stagnation point flow nanofluid over a surface with convective boundary conditions. Comm. Nonlinear Sci. Num. Simulat. **17**, 4210–4223 (2012)
13. Narayana, M., Sibanda, P.: Laminar flow of a nanofluid over an unsteady streching sheet. Int. J. Heat Mass Transfer **55**, 7552–7560 (2012)
14. Ibrahim, W., Shankarand, B., Nandepponavar, M.M.: MHD stagnation point flow and heat transfer due to nanofluid towards a stretching sheet. Int. J. Heat Mass Transfer **56**, 1–9 (2013)
15. Rashidi, M.M., Anwar, O., Asadi, M., Rastegari, M.T.: DTM-Pade modelling of natural convective boundary layer flow of a nanofluid past a vertical surface. Int. J. Thermal Enviorment Eng **4**, 13–24 (2012)
16. Turkyilmazoglu, M., Pop, I.: Heat and mass transfer of unsteady natural convection flow of some nanofluids past a vertical infinite flat plate with radiation effect. Int. J. Heat Mass Transfer **59**, 167–171 (2013)
17. Sheikholeslami, M., Hatam, M., Ganji, D.D.: Heat flux boundary condition for nanofluid filled enclosure in presence of magnetic field. J. Molecular Liquids **190**, 112–120 (2014)
18. Turkyilmazoglu, M., Ashorynejad, H.R., Sheikholeslami, M., Pop, I., Ganji, D.D.: Nanofluid flow and heat transfer due to a stretching cylinder in the presence of magnetic field. Int. J. Heat Mass Transfer **49**, 427–436 (2013)
19. Turkyilmazoglu, M.: Unsteady convection flow of some nanofluids past a moving vertical flat plate with heat transfer, ASME. J. Heat Transfer **136**, 031704 (2013)
20. Khan, W.A.: Boundary-layer flow of a nanofluid past a stretching sheet. Int. J. Heat Mass Transfer **53**, 2477–2483 (2010)

21. Nield, D.A., Kuznetsov, A.V.: The Cheng-Minkowycz problem for natural convective boundary-layer flow in a porous medium saturated by a nanofluid. Int. J. Heat Mass Transfer **52**, 5792–5795 (2009)
22. Kuznetsov, A.V., Nield, D.A.: Natural convective boundary-layer flow of a nanofluid past a vertical plate. Int. J. Therm. Sci. **49**, 243–247 (2010)
23. Gorder, R.A.V., Sweet, E., Vajravelu, K.: Nano boundary layers over stretching surfaces. Commun. Nonlinear Sci. Numm. Simulat. **15**, 1494–1500 (2010)
24. Liao, S.J.: A kind of approximate solution technique which does not depend upon small parameters (II)- An application in fluid mechanics. Int. J. Nonlinear Mech. **32**, 815–822 (1997)
25. Liao, S.J.: An optimal homotopy analysis approach for strongly nonlinear differential equations. Commun. Nonlinear Sci. Numm. Simulat. **15**, 2315–2332 (2010)
26. Ghoreishi, M., Ismail, A.I.B.Md., Alomari, A.k., Bataineh, A.S.: The comparison between homotopy analysis method and optimal homotopy asymtotic method for nonlinear age structured population models. Commun. Nonlinear Sci. Numm. Simulat. **17**, 1163–1177 (2012)
27. Gorder, R.A.V.: Control of error in the homotopy analysis of semi-linear elliptic boundary value problems. Numer. Algoritm. **61**, 613–629 (2012)
28. Tao, F., You, X.C.h.: Optimal homotopy analysis method for nonlinear differential equations in the boundary layer. Numer. Algoritm. **62**, 337–354 (2013)
29. Zhao, N., Wang, C.: A one-step optimal homotopy analysis method for nonlinear differential equations. Commun. Nonlinear Sci. Numm. Simulat. **15**, 2026–2036 (2010)
30. Mallory, K., Gorder, R.A.V.: Optimal homotopy analysis and control of error for solution to the non-local Whitham equation. Numer. Algoritm. **66**, 843–863 (2013)
31. Liao, S.J.: Beyond perturbation: Introduction to the homotopy analysis method. Chapman and Hall/CRC Press, Boca Raton (2003)
32. Liao, S.J.: Homotopy analysis method in non-linear differential equations. Higher education press, Beijing (2012)
33. Farooq, U., Liang, L.Z.: Non-linear heat transfer in a two layer flow with nanofluids by OHAM, ASME. J. Heat Mass Transfer **2**(136) (2014). doi:10.1115/1.4025432
34. Liao, S.J.: Notes on the homotopy analysis method- Some defnitions and theorems. J. Commun. Nonlinear Sci. Nummer. Simulat. **14**, 983–997 (2009)